

Properties of radiation defects and threshold energy of displacement in zirconium hydride obtained by new deep-learning potential

Xi Wang(王玺), Meng Tang(唐孟), Ming-Xuan Jiang(蒋明璇), Yang-Chun Chen(陈阳春), Zhi-Xiao Liu(刘智骁), and Hui-Qiu Deng(邓辉球)

Citation: Chin. Phys. B, 2024, 33 (**7**): 076103. DOI: 10.1088/1674-1056/ad362b
Journal homepage: http://cpb.iphy.ac.cn; http://iopscience.iop.org/cpb

What follows is a list of articles you may be interested in

Controlled thermally-driven mass transport in carbon nanotubes using carbon hoops

Yaolong Li(李耀隆), Songyuan Li(李松远), Meifen Wang(王美芬), and Renliang Zhang(张任良)
Chin. Phys. B, 2024, 33 (**4**): 046101. DOI: 10.1088/1674-1056/ad14ff

Molecular dynamics study of primary radiation damage in TiVTa concentrated solid-solution alloy

Yong-Peng Zhao(赵永鹏), Yan-Kun Dou(豆艳坤), Xin-Fu He(贺新福), Han Cao(曹晗),Lin-Feng Wang(王林枫), Hui-Qiu Deng(邓辉球), and Wen Yang(杨文)
Chin. Phys. B, 2024, 33 (**3**): 036104. DOI: 10.1088/1674-1056/ad0146

Electronic effects on radiation damage in α-iron: A molecular dynamics study

Lin Jiang(江林), Min Li(李敏), Bao-Qin Fu(付宝勤), Jie-Chao Cui(崔节超), and Qing Hou(侯氢)
Chin. Phys. B, 2024, 33 (**3**): 036103. DOI: 10.1088/1674-1056/ad0ec4

Anelasticity to plasticity transition in a model two-dimensional amorphous solid

Baoshuang Shang(尚宝双)
Chin. Phys. B, 2024, 33 (**1**): 016102. DOI: 10.1088/1674-1056/acf82c

Classification and structural characteristics of amorphous materials based on interpretable deep learning

Jiamei Cui(崔佳梅), Yunjie Li(李韵洁), Cai Zhao(赵偲), and Wen Zheng(郑文)
Chin. Phys. B, 2023, 32 (**9**): 096101. DOI: 10.1088/1674-1056/acd7d0

Properties of radiation defects and threshold energy of displacement in zirconium hydride obtained by new deep-learning potential

Xi Wang(王玺)[1], Meng Tang(唐孟)[1], Ming-Xuan Jiang(蒋明璇)[1], Yang-Chun Chen(陈阳春)[2], Zhi-Xiao Liu(刘智骁)[2,†], and Hui-Qiu Deng(邓辉球)[1,‡]

[1] *School of Physics and Electronics, Hunan University, Changsha* 410082, *China*
[2] *College of Materials Science and Engineering, Hunan University, Changsha* 410082, *China*

(Received 3 February 2024; revised manuscript received 15 March 2024; accepted manuscript online 21 March 2024)

Zirconium hydride (ZrH_2) is an ideal neutron moderator material. However, radiation effect significantly changes its properties, which affect its behavior and the lifespan of the reactor. The threshold energy of displacement is an important quantity of the number of radiation defects produced, which helps us to predict the evolution of radiation defects in ZrH_2. Molecular dynamics (MD) and *ab initio* molecular dynamics (AIMD) are two main methods of calculating the threshold energy of displacement. The MD simulations with empirical potentials often cannot accurately depict the transitional states that lattice atoms must surpass to reach an interstitial state. Additionally, the AIMD method is unable to perform large-scale calculation, which poses a computational challenge beyond the simulation range of density functional theory. Machine learning potentials are renowned for their high accuracy and efficiency, making them an increasingly preferred choice for molecular dynamics simulations. In this work, we develop an accurate potential energy model for the ZrH_2 system by using the deep-potential (DP) method. The DP model has a high degree of agreement with first-principles calculations for the typical defect energy and mechanical properties of the ZrH_2 system, including the basic bulk properties, formation energy of point defects, as well as diffusion behavior of hydrogen and zirconium. By integrating the DP model with Ziegler–Biersack–Littmark (ZBL) potential, we can predict the threshold energy of displacement of zirconium and hydrogen in ε-ZrH_2.

Keywords: zirconium hydride, deep learning potential, radiation defects, molecular dynamics, threshold energy of displacement

PACS: 61.66.Dk, 07.05.Mh, 34.20.Cf, 82.20.Wt **DOI:** 10.1088/1674-1056/ad362b

1. Introduction

Zirconium hydride is commonly used as a neutron moderator in nuclear reactors.[1] The TRIGA research reactor[2] of general atomics and the thermonuclear propulsion project[3] of NASA both used zirconium hydride as the neutron moderator material. There have been many experimental[4–8] and theoretical[9–15] studies on zirconium hydride. The experimental researches primarily focused on the location of hydrogen in α-Zr,[4,5] the phase stability of zirconium hydride in zircaloy,[6] and identification and characterization of zirconium hydrides,[7] as well as the effect of hydride precipitation on mechanical properties of zircaloy-4 panels with and without notches.[8] The density functional theory was employed to theoretically examine fundamental characteristics of the zirconium hydride system, including its ground state crystal structure,[15] the influence of hydrogen concentration and position on phase stability,[10,11] as well as to explore the thermodynamic properties[13,14] and predict potential structures.[12]

The investigation into the resistance of zirconium hydride to neutron radiation and elucidation of its radiation damage mechanism are among the focal areas of research. Zirconium hydride serves as a neutron moderator in extreme operating environments of high temperature and intense radiation in nuclear reactors: fission neutrons collide with zirconium hydride lattice atoms to generate a large number of primary recoil atoms carrying energy, thus triggering off a shift cascade and generating primary damage defects such as vacancies and interstitial atoms. These defects diffuse and aggregate to form defect structures such as dislocation loops and voids, thereby changing the microstructure and macroscopic performance of zirconium hydride, affecting its service behavior and reactor life. Due to the complexity of experimental conditions, it is difficult to observe the influence of defect properties on the microstructure and service performance of zirconium hydride experimentally. The molecular dynamics method based on interatomic potentials is an effective tool for addressing the challenges mentioned above. This method enables dynamic simulations of millions of atoms at high temperatures, with a time scale reaching the nanosecond level. However, the accuracy of these methods largely depends on the ability of interatomic potentials to accurately describe the material properties. Currently, the attention of researchers is paid to the diffusion behavior of hydrogen in α-Zr by using the embedded-atom method (EAM)[16] and the modified embedded-atom

[†]Corresponding author. E-mail: zxliu@hnu.edu.cn
[‡]Corresponding author. E-mail: hqdeng@hnu.edu.cn

© 2024 Chinese Physical Society and IOP Publishing Ltd

method (MEAM)[17] potentials. However, these potentials are not suitable for simulating hydrides. The charge-optimized many-body (COMB) potential,[18] which focuses on zirconium hydride (ZrH_2), cannot describe δ-ZH_2 or ε-ZrH_2 simultaneously. Similarly, the MEAM potential[19] specifically addresses the diffusion of hydrogen in δ-ZH_2. Due to the intricate phase structure of zirconium hydride, the accurate describing of the zirconium hydride system using traditional empirical potential poses significant challenges. The latest developments of machine learning (ML) potential[20–30] methods bring new possibilities to high-precision atomic interaction modeling. After appropriate training, these models may achieve high accuracy comparable to density functional theory (DFT) methods. Deep-potential (DP), one of the popular machine learning potential methods, has demonstrated strong ability to describe the properties of multi-component materials due to the ability of neural networks to excellently fit high-dimensional and multi-variable functions. The DP method has been successfully applied to various metal material fields, including Al–Mg alloys,[31] Al–Cu–Mg alloys,[32] Ag–Au nanoalloys,[33] Ti,[34] V,[35] W,[36] and Fe–He[37] systems. Therefore, it is anticipated that the DP method can be employed to construct a machine learning potential for the ZrH_2 system, enabling atomic simulations and facilitating the exploration of the effects of radiation on the mechanism of zirconium hydride. The purpose of this work is to develop a specific interatomic potential by using the deep-potential method of the ZrH_2 system, capable of accurately describing the properties of both zirconium and zirconium hydride. The prediction of threshold energy of displacement in ε-ZrH_2 can provide preliminary preparation for the molecular dynamics study of the radiation defects of ZrH_2.

2. Methods

2.1. Deep learning potential model

The DP[29] model divides the total potential energy of the system into the sum of energy of each atomic configuration, i.e., $E = \sum E_i$, where E_i is determined by the local environment of atom i within the truncation radius R_c. The mapping relationship between E_i and the atomic local environment includes the multi-body interactions among atoms. The local environment can be defined as $\{j | j \in N_{R_c}(i)\}$, where j represents the atoms within the cutoff radius of atom i. The total number of atoms within the cutoff radius is $N_i = |N_{R_c}(i)|$, and the local environment matrix of atom i can be expressed as

$$\begin{aligned} &\Re^i = \left\{R_{1i}^{\mathrm{T}}, \ldots, R_{ji}^{\mathrm{T}}, \ldots R_{N_i,i}^{\mathrm{T}}\right\}\left\{R_{1i}^{\mathrm{T}}, \ldots, R_{ji}^{\mathrm{T}}, \ldots R_{N_i,i}^{\mathrm{T}}\right\}^{\mathrm{T}}, \\ &R_{ji} = (x_{ji}, y_{ji}, z_{ji}), \end{aligned} \tag{1}$$

where $R_{ji} = R_j - R_i$ is relative coordinate. In the DP model, the local environment matrix is initially transformed into a descriptor D that maintains the symmetries of rotation, translation, and permutation. Then, the energy E_i is mapped by using the fitting net F and expressed as

$$E_i = F\left(D\left(\Re^i\right)\right). \tag{2}$$

The DP model comprises two neural networks: one is for embedding and the other is for fitting. Elaborate parameter configurations for the embedding layer and fitting layer are delineated in Subsection 2.2.4.

2.2. Sampling scheme based on DP-GEN

The DP-GEN[38] active learning process comprises three main steps: exploration, labeling, and training. Beginning with an initial training set, the potential is trained and utilized to explore spatial structure through a molecular dynamics approach. Simultaneously, the error exploration indicator with the largest internal bias is employed to filter out configurations that cannot be accurately predicted, which are then sent for labeling. The energy, force, and virial tensors of nominal configurations are computed by using first-principles software and added to the training set for further potential refinement. These three processes form a cyclic loop where the initial training set generates potentials used in exploring spatial structures via molecular dynamics methods, resulting in a wide range of current configurations. This cycle repeats until all explored spaces can be accurately described, leading to the development of a comprehensive and precise model of the potential.

2.2.1. Initial dataset

The research conducted by Zheng *et al.*[39] demonstrates that zirconium hydride undergoes a gradual transition from the hcp phase to the fcc phase (δ phase) and ultimately to the fct phase (ε phase) as hydrogen concentration increases. In this study, we consider three phases. For zirconium, we selecte α-Zr with a hexagonal closed packet (hcp) crystal structure and $P63/mmc$ space group as the initial configuration. As for zirconium hydride, we chose ZrH_2 in its common and stable form with $I4/mmm$ symmetry (#139 space group) as the ε phase (Fig. 1(a)), and ZrH_2 with $Fm3m$ symmetry (#225 space group) as the δ phase (Fig. 1(b)). It is worth noting that for the lattice problem of ε-ZrH_2 with $I4/mmm$ symmetry, we adopt lattice constants of $a = b = 3.538$ Å, $c = 4.406$ Å, and $c/a = 1.25$ in line with the data presented by Zhu *et al.*[40] and Chattaraj *et al.*[41]

In this work, the initial structure comprises three optimized phases (α-Zr, δ-ZH_2, ε-ZrH_2) with random perturbations. To induce perturbation, strain is applied to the lattice constant of the optimized structure in increments of 1% ranging from 98% to 102%. Additionally, random perturbations are introduced into both atomic positions and box sizes.

The maximum displacement for atomic positions is limited to 0.01 Å, while the allowable maximum variation for the box shape is set to 3%. The resulting perturbed structures serve as initial configurations for *ab initio* molecular dynamics (AIMD)[42] simulations conducted at a temperature of 100 K. The obtained results are then labeled with energy, force, virial tensor, element information, box size information, and atomic position information to form the initial training set. Notably, all training sets are labeled with the above six pieces of information.

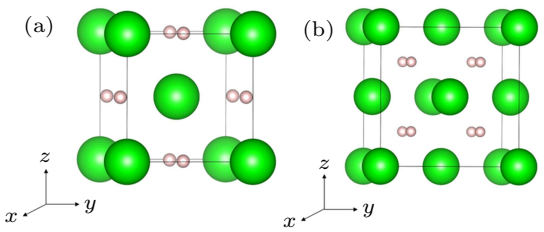


Fig. 1. Structures of ZrH_2: (a) ε phase and (b) δ phase.

2.2.2. Exploration

In this work, the configuration was explored by DP-based molecular dynamics (Deepmd) using the LAMMPS package,[43] which is compiled with support from the DeePMD-kit.[44] Since zirconium hydride and zirconium have different strategies for exploring configurations, zirconium hydride and zirconium are sampled separately. For zirconium, the initial configuration consists of a randomly perturbed HCP configuration of 3×3×3 supercells. The NVT ensemble molecular dynamics simulations are performed over a range of thermodynamic states spanning from 50 K to 1000 K, encompassing the temperature at which α-Zr transforms into β-Zr. For zirconium hydride, the initial configuration consists of randomly perturbed δ-ZH_2 and ε-ZrH_2 of 2×2×2 supercells. The isothermal–isobaric (NPT) ensemble molecular dynamics simulations are performed in a range of thermodynamic states, spanning from 50 K to 1000 K (the temperature at which ε-ZrH_2 remains stable), and pressures ranging from 1 bar to 5×10^5 bar (1 bar = 10^5 Pa). The permissible range for the deviation of atomic forces is defined as the range from 0.05 eV/Å to 0.30 eV/Å. These two values, 0.05 eV/Å and 0.30 eV/Å, are determined by referring to the model deviation of the potential trained by using the initial training set. The iteration process involves constant adjustments of these values until it proceeds effectively.

2.2.3. Labeling

The calculation of the training set required for the DP model is based on the DFT[45,46] with the generalized-gradient approximation (GGA) proposed by Perdew, Burke, and Ernzerhof (PBE)[47] for the exchange–correlation functional. First-principles calculations are performed by the Vienna *ab initio* simulation package[48,49] (VASP5.4.4). The *k*-point meshes for Brillouin zone sampling are constructed by using the Monk–Horst–Pack scheme with a grid spacing of 0.15 $Å^{-1}$. The plane-wave energy cutoff of the plane-wave basis set is set to 600 eV. For Zr, electron descriptions corresponding to the $4d^25s^2$ valence states are employed, while only the $1s^1$ electron is treated for H. In the process of an atomic structure optimization, when the energy change between the two electrons self-consistent steps is less than 10^{-6} eV, and all forces after the ion step are less than 0.01 eV/Å, convergence is assumed.

2.2.4. Training

During the DPGEN iteration, each iteration trains the four DP models by using the same training set and the same training parameters. Both the embedded neural network and the fitted neural network have three layers of neural networks, with the size of the embedded neural network being (25,50,100), and the size of the fitted neural network (240,240,240). The embedded neural network cutoff radius of zirconium hydride and zirconium are both set to 6 Å. The number of training steps is set to 4×10^6, and the learning rate decreases exponentially from 1×10^{-3} to 3.5×10^{-8}. The starting prefactors of energy, force, and virial (p_ε, p_f, p_ξ) are set to 0.02, 1000, and 0, respectively.

2.3. Long training

After completing the DPGEN iteration, the final training set is composed of the training set obtained through iterations and the self-provided training set. The efficient model is trained with 1.6×10^7 steps. The number of initial configurations, the number of DP-GEN samples of ZrH_2, the number of point defects datasets, the number of the hydrogen molecular, and the number of CI-NEB datasets are all listed in Table 1. Among them, the hydrogen molecular training set is the result of the optimization of hydrogen molecules at different distances in 10 Å×10 Å×10 Å supercells. The DP-GEN iteration produces detailed data, which are available in the supporting information. We employ the single-point energy calculation and AIMD method to acquire precise data on point defects.

Table 1. Number and proportion of training sets.

	Dataset type	Number of datasets	Weightage (%)
δ-ZH_2	initialization datasets	3000	10.9
	DP-GEN bulk of δ-ZH_2	1755	6.4
	points defects datasets	4236	15.3
	CI-NEB datasets	2800	10.1
ε-ZrH_2	initialization datasets	2581	9.3
	DP-GEN bulk of ε-ZrH_2	2760	9.9
	points defects datasets	3907	14.2
	CI NEB datasets	1785	6.5
α-Zr	initialization datasets	3000	10.9
	DP-GEN bulk of α-Zr	1199	4.3
	DP-GEN surface	492	1.8
H_2	hydrogen molecules	100	0.4

The embedded neural network cutoff radius of zirconium hydride and zirconium are both set to 8 Å. The learning rate decreases from 1×10^{-3} to 3.2×10^{-8}. The starting perfectors of p_ε, p_f, p_ξ are set to 0.02, 1000, and 100, respectively. During retraining, the training step is set to 4×10^5 steps, to inherit the knowledge learned from the old model, the learning rate is lowered by an order of magnitude to 10^{-4}, and the starting values of p_ε, p_f, p_ξ are set to 100, 1, 0.9, respectively. The root-means-square error (RMSE) of the energy (normalized by the number of atoms), the atomic forces, and the virial tensor (normalized by the number of atoms) in the entire training dataset are 2.562×10^{-3} eV/atom, 5.402×10^{-2} eV/Å, and 3.756×10^{-1} eV/atom, respectively.

3. Results

3.1. Basic physical properties

To validate the accuracy of the current DP model, we initially examine the fundamental bulk properties of α-Zr, δ-ZrH_2, and ε-ZrH_2. The obtained results are subsequently compared with the values derived from DFT, experiments, or calculations conducted by using other interatomic potential models. For α-Zr, the lattice parameters (a and c), bulk modulus (B), elastic constants (C_{11}, C_{12}, C_{13}, C_{33}, and C_{44}), and surface energy (surf-0001, surf-10$\bar{1}$1, surf-11$\bar{2}$2) are listed in Table 2.

Table 2. Calculated lattice constants (a and c/a), elastic constants (C_{11}, C_{12}, C_{44}, C_{13}, and C_{33}), bulk modulus (B), and surface energy (surf-0001, surf-10$\bar{1}$0, surf-11$\bar{2}$2) of α-Zr, with surface formation energy being in units of J·m^{-2}.

Properties	DP (present)	DFT (present)	Exp.	DFT	NNP[51]	EAM[50]
a (HCP)	3.241	3.239	3.231[57]	3.231[58]	3.231	3.223
c/a	1.597	1.599	1.603[57]	1.598[58]	1.602	1.598
B	95.80	94.82				111.6
C_{11}	143.94	148.04	155.4[59]	147.78[58]	141.5	157.3
C_{12}	69.75	62.24	67.2[59]	70.66[58]	67.2	98.9
C_{13}	69.37	65.54	64.6[59]	65.51[58]	67.2	77.6
C_{33}	159.33	170.01	172.5[59]	168.29[58]	168.7	181.4
C_{44}	26.24	24.61	36.3[59]	25.41[58]	28.9	30.3
Surf-0001	1589.45	1638.12	2000[60]	1580[51]	1593.8	1127
Surf-10$\bar{1}$0	1657.40	1662.25	2050[61]	1664[51]	1631.9	1273
Surf-11$\bar{2}$2	1724.48	1718.34				

In general, the results from the DP model are in better agreement with the DFT results for these properties in comparison with those from EAM[50] and demonstrate that its performance is comparable to NNP's[51] in terms of DFT results. The lattice constants are well-matched by all three potentials in comparison with the DFT calculation. However, due to the inherent differences between the experimental results and DFT calculations, some disparities also exist. As mentioned in Refs. [52–56], the DFT results of C_{33} and C_{44} are slightly lower than the experimental values, and the results from the DP model are consistent with DFT results, which are naturally lower than the experimental values. The limitations of the DP model itself and the disparities between experimental environments and simulations are the primary factors that contributs to this scenario. The lowest energy surface predicted by the DP model is surf-0001, consistent with the results of DFT and Ref. [51], and the DP model has high accuracy for surfaces (surf-10$\bar{1}$1) and (surf-11$\bar{2}$2). The DP model shows that the surface energy is consistent with the DFT result, and can also predict the energy order of the surface of zirconium. Generally, the EAM potential does not include the surface energy in the fitting target, so the EAM potential does not behave as well as the DP model or the NNP in terms of surface energy. The DP model demonstrates satisfactory performance in predicting the bulk properties of α-Zr, as indicated by the above results.

For δ-ZrH_2, the result of the optimized lattice constants and elastic constants together with previous theoretical results are given in Table 3.

Table 3. Calculated values of lattice constant (a), and elastic constants (C_{11}, C_{12}, C_{44}) of δ-ZrH_2.

Properties	DP (present)	DFT (present)	DFT[39]	MEAM
a	4.821	4.821	4.824	4.620[19]
B	133.05	132.94	132.92	142[19]
C_{11}	96.03	79.427	78.06	82.40*
C_{12}	151.56	156.081	160.35	104.37*
C_{44}	–26.06	–35.831	–39.42	–16203.46*

*Calculated in the present work.

Our calculated results exhibit excellent concordance with other theoretical values. The values for C_{44} and the C_{11}–C_{12} calculated by DFT are negative, indicating mechanical instability of δ-ZrH_2 at zero temperature.

For ε-ZrH_2, the results are shown in Table 4. From the the perspective of elastic performance, unlike δ-ZrH_2, ε-ZrH_2 meets the mechanical stability conditions and remains stable at a temperature of 0 K. The DP model is demonstrated to exhibit satisfactory agreement with DFT in a wide range of properties, including elastic constants (C_{11}, C_{12}, C_{13}, C_{33}, and C_{44}), lattice constants (a, c), as well as bulk modulus (B).

Table 4. Calculated values of lattice constants, elastic constants (C_{11}, C_{12}, C_{13}, C_{33}, and C_{44}), bulk modulus of ε-ZrH_2.

Properties	DP (present)	DFT (present)	Exp.	DFT
a	3.538	3.541	3.518[62]	3.538[41]
c	4.446	4.450	4.447[62]	4.442[41]
c/a	1.256	1.256	1.264[62]	1.255[41]
B	134.60	133.16		132*
C_{11}	225.15	216.44		225*
C_{12}	94.84	100.64		91*
C_{13}	102.65	102.06		105*
C_{33}	161.28	152.2		148*
C_{44}	31.07	40.95		32*

*Cited from Materials Project Database.

Further, we verify the tendency of the energy variation with the equilibrium volume in the DP model. Using the DP-GEN workflow, we investigate the energy change with volume at 80% to 120% of the equilibrium volume of ZrH_2 and α-Zr. We calculate the equations of state (EOSs) of three EAM potentials of Mendelev and Ackland,[16] which are denoted as Mendelev and Ackland #1, #2, #3 respectively. Unlike the empirical potential where the energy of a single isolated atom is zero, the energy of a single isolated atom in the DP model is not zero. To make a better comparison of EOS among different potentials of α-Zr, we use cohesive energy as a function of the change of DFT and potential energy with atomic volume. For ZrH_2, we only compare the DFT results with the EOS predicted by the DP model.

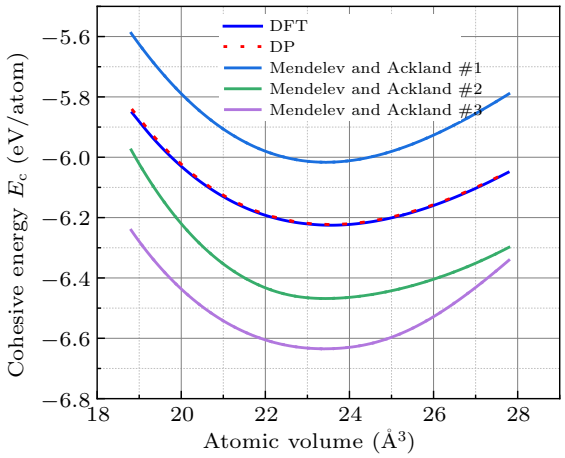


Fig. 2. Plots of cohesive energy versus α-Zr in atomic volume ranging from 18 Å^3 to 28 Å^3.

As depicted in Fig. 2, the DP model shows excellent agreement with our DFT calculation for α-Zr. The discrepancy in the EOS calculated by the EAM and DP models can be ascribed to their distinct predictions regarding the lattice parameter. When the volume is smaller than the equilibrium volume, the energy of the Mendelev and Ackland #2 exhibits a more pronounced increase than the DFT calculation. A faster growth of the energy of Mendelev and Ackland #1 is also noticed as the system is larger than the equilibrium volume. Compared with the EAM potential, the DP model exhibits good agreement with the EOS obtained from DFT calculations. The main difference is due to different predictions of lattice constants by DP model and EAM potential.

In the volume change range of ZH_2, regardless of δ-ZH_2 or ε-ZrH_2 (Figs. 3 and 4), there is a strong consistency between the DP model and DFT. The EOS for δ-ZH_2 shows negligible differences from DFT predictions, while ε-ZrH_2 exhibits slight variations in compression volume, gradually aligning with DFT predictions. These findings highlight the sensitivity of the DP model to energy change and its high precision, thereby offering promising prospects for achieving accurate MD simulations in large-scale systems.

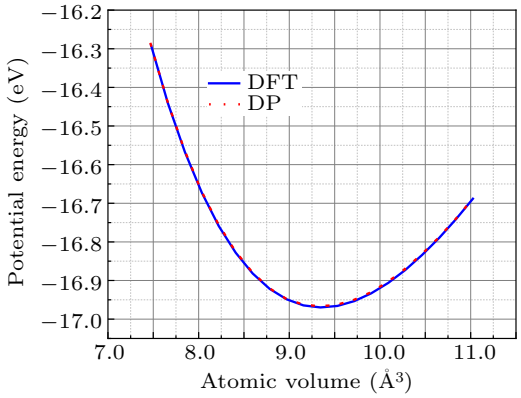


Fig. 3. Potential energy versus atomic volume ranging from 7 Å^3 to 11 Å^3 of δ-ZrH_2.

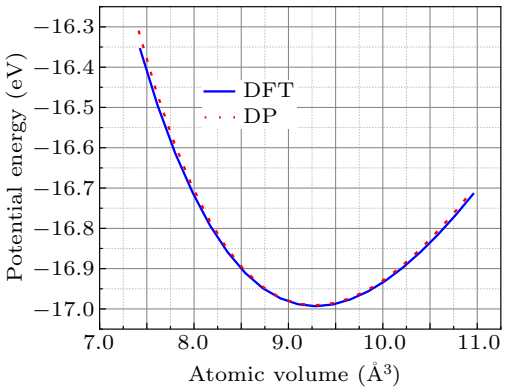


Fig. 4. Plot of potential energy versus atomic volume ranging from 7 Å^3 to 11 Å^3 of ε-ZrH_2.

3.2. Formation energy of point defects in ZrH_2

In the radiation environment, point defects will occur frequently, and defect clusters will be formed to a certain extent, which will directly affect the thermodynamic properties. At the same time, point defect is an important index to measure potential quality. In this work, we fully consider various point defects in ZrH_2. The values of formation energy of self-interstitial atom (SIA) and single vacancy atom are shown in Tables 5 and 6. For δ-ZH_2 and ε-ZrH_2, we consider the values of formation energy of H at the octahedral interstitial sites of Zr (H_δ^{Oct} and H_ε^{Oct}), Zr at octahedral interstitial position of Zr (Zr_δ^{Oct} and Zr_ε^{Oct}), a single H vacancy (H_δ^{Vac} and H_ε^{Vac}), a single Zr vacancy (Zr_δ^{Vac} and Zr_ε^{Vac}), and hydrogen atom from

the tetrahedral position of zirconium to the octahedral position of zirconium (Frenkel-pair). The vacancy calculation equation is as follows:

$$E_v^{\mathrm{f}} = E_v - E_{\mathrm{perfect}} + E_{\mathrm{soild}}^{\mathrm{Zr}}(E_{\mathrm{gas}}^{\mathrm{H}}). \tag{3}$$

The SIA calculation equation is as follows:

$$E_{\mathrm{f}}^{\mathrm{SIA}} = E_{\mathrm{perfect+Zr(H)}} - E_{\mathrm{perfect}} - E_{\mathrm{soild}}^{\mathrm{Zr}}(E_{\mathrm{gas}}^{\mathrm{H}}), \tag{4}$$

in which E_{perfect}, $E_{\mathrm{soild}}^{\mathrm{Zr}}$, $E_{\mathrm{gas}}^{\mathrm{H}}$, E_v, $E_{\mathrm{perfect+Zr(H)}}$ represent the total energy of the perfect ZrH_2 supercell, solid Zr crystal, gas hydrogen, vacancy defect, self-interstitial defect. For δ-ZH_2, it can be seen from the calculation that the octahedral interstitial position of zirconium (H_δ^{Oct}) can form hydrogen atom defect in δ-ZH_2 most easily and it has a minimum energy of 0.383 eV. Conversely, the most difficult defect to form is Zr_δ^{Oct}, which has the largest formation energy of 6.261 eV. The DP model has the same result as the DFT for the energy order of the formation energy of each defect, both being $H_\delta^{\mathrm{Oct}} < H_\delta^{\mathrm{Vac}} < \delta$-Frenkel-pair $< Zr_\delta^{\mathrm{Vac}} < Zr_\delta^{\mathrm{Oct}}$. Overall, the DP model has satisfactory results in terms of the performance of defect formation energy.

Table 5. Calculation results of point defects of δ-ZrH_2, covering vacancy formation energy of H and Zr (H_δ^{Vac}, Zr_δ^{Vac}), defect formation energy of H and Zr at octahedral interstitial sites ($H_\delta^{\mathrm{Oct}}Zr_\delta^{\mathrm{Oct}}$), defect formation energy of H from tetrahedral position of zirconium to octahedral position of zirconium (δ-Frenkel-pair), in units of eV.

Type	DFT (present)	DP (present)
H_δ^{Oct}	0.383	0.358
H_δ^{Vac}	0.835	0.818
Zr_δ^{Oct}	6.261	6.181
Zr_δ^{Vac}	2.064	2.022
δ-Frenkel-pair	1.214	1.156

Table 6. Calculation results of point defects of ε-ZrH_2, covering vacancy formation energy of H and Zr ($H_\varepsilon^{\mathrm{Vac}}$, $Zr_\varepsilon^{\mathrm{Vac}}$), defect formation energy of H and Zr at octahedral interstitial sites ($H_\varepsilon^{\mathrm{Oct}}Zr_\varepsilon^{\mathrm{Oct}}$), defect formation energy of H from tetrahedral position of zirconium to the octahedral position of zirconium (ε-Frenkel-pair), in units of eV.

Type	DFT (present)	DP (present)
$H_\varepsilon^{\mathrm{Oct}}$	0.447	0.416
$H_\varepsilon^{\mathrm{Vac}}$	0.846	0.836
$Zr_\varepsilon^{\mathrm{Oct}}$	6.152	6.120
$Zr_\varepsilon^{\mathrm{Vac}}$	2.552	2.527
ε-Frenkel-pair	1.234	1.202

For ε-ZrH_2, from the DFT calculations it can follow that the results of each hydrogen defect have relatively consistent results with δ-ZrH_2, such as $H_\varepsilon^{\mathrm{Vac}}$ and ε-Frenkel-pair results are consistent with H_δ^{Vac} and δ-Frenkel-pair, $H_\varepsilon^{\mathrm{Oct}}$ and H_δ^{Oct} have similar results. This can be related to the arrangement of hydrogen occupying the tetrahedral position of the zirconium in both δ-ZH_2 and ε-ZrH_2. The performance of the DP model is also encouraging in the defect formation energy of ε-ZrH_2, and the error of DFT is within 50 meV. The precise characterization of defect properties by the DP model contributes to accurate determination of the threshold energy of displacement and investigation into the generation and evolution of radiation defects under radiation conditions.

3.3. Diffusion of hydrogen and zirconium in ZrH_2

To further explore the diffusion behaviors of H defects and Zr defects in ZrH_2, the climbing image nudged elastic band (CI-NEB)[63] method is used to identify the transition state. We consider three different migration paths in δ-ZrH_2 and ε-ZrH_2, hydrogen atom migration between octahedral gaps of zirconium ($H_\delta^{\mathrm{Oct-Oct}}$, $H_\varepsilon^{\mathrm{Oct-Oct}}$), migration of hydrogen atom in the presence of hydrogen vacancy ($H_\delta^{\mathrm{Vac-Vac}}$, $H_\varepsilon^{\mathrm{Vac-Vac}}$) and migration of zirconium atom in the presence of zirconium vacancy ($Zr_\delta^{\mathrm{Vac-Vac}}$, $Zr_\varepsilon^{\mathrm{Vac-Vac}}$). Our objective is to enhance the learning capability of the DP model by incorporating a wide range of migration paths, ensuring a comprehensive training dataset, and identifying the migration path with the lowest energy and most likely migration path. For δ-ZrH_2, various migration paths in the [001] direction are shown in Fig. 5, $H_\delta^{\mathrm{Oct-Oct-1}}$ is that the hydrogen atom starts from the octahedral position to the octahedral position of the same plane, $H_\delta^{\mathrm{Oct-Oct-2}}$ is that hydrogen atom starts from the octahedron position to the lower atom, and the lower hydrogen atom reaches the octahedral site of the same plane.

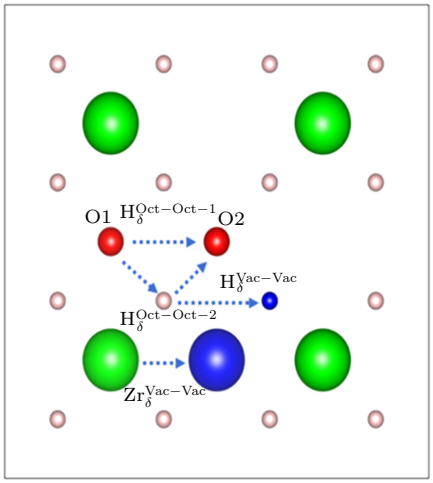


Fig. 5. Diagram of δ-ZrH_2 diffusion model within (001) plane. Both red and gray balls represent hydrogen atoms, with the red ones situated at octahedral interstitial sites. The green ball denotes zirconium atom, and blue balls refer to vacancies. Dashed lines show diffusion paths.

The $H_\delta^{\mathrm{Vac-Vac}}$ path is the hydrogen atom arriving at the vacancy, leaving a new vacancy. and $Zr_\delta^{\mathrm{Vac-Vac}}$ is the same as $H_\delta^{\mathrm{Vac-Vac}}$, except that the moving atom is zirconium. For ε-ZrH_2, various migration paths of ε-ZrH_2 in the [001] direction are shown in Fig. 6. Like δ-ZrH_2, $Zr_\varepsilon^{\mathrm{Vac-Vac}}$ is the closest neighbors of atom moving to the same plane. The $H_\varepsilon^{\mathrm{Vac-Vac}}$ is the atom moving to closest neighbors of the upper plane. The

$H_{\varepsilon}^{Oct-Oct}$ is that hydrogen atom starts from the octahedral site to the octahedral site on the same plane.

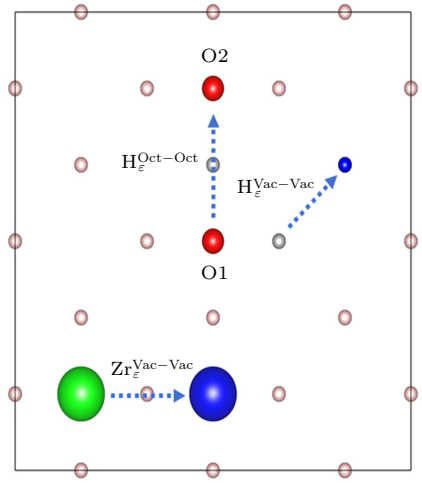


Fig. 6. Diagram of ε-ZrH_2 diffusion model within (001) plane. Both red and gray balls represent hydrogen atoms, with red ones situated at octahedral interstitial sites. Green ball denotes zirconium atom, and blue ones refer to vacancies. Dashed lines show diffusion paths.

In the NEB calculation of VASP, we insert five points in each transition path of δ-ZrH_2 and three points in ε-ZrH_2, based on the optimized atomic distances of the initial state and final state. The NEB method in LAMMPS is also used to verify the accuracy of the DP model for the migration barrier. Similarly, to accurately verify the performance of the DP model on the migration barrier, the insertion points in the middle of LAMMPS are consistent with DFT calculations. When the maximum interatomic force is less than 0.01 eV/Å, the NEB calculation is considered to be convergent. The time step for subsequent molecular dynamics simulations is set to 0.001 ps. Figures 7 and 8 depict the energy curves for different paths, with the highest peaks being the diffusion and migration barriers of migrating atoms.

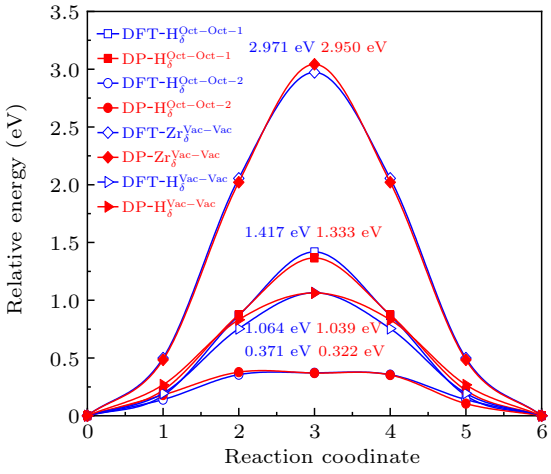


Fig. 7. Migration energy along different paths in δ-ZrH_2. $H_{\delta}^{Oct-Oct-1}$ refers to the NEB pathway for a hydrogen atom migrating from an octahedral site to another octahedral site. $H_{\delta}^{Oct-Oct-2}$ represents the pathway for a hydrogen atom to migrate from a tetrahedral site to an octahedral site. $H_{\delta}^{Vac-Vac}$ denotes the pathway of a hydrogen atom migrating from a tetrahedral site to a tetrahedral vacancy site. $Zr_{\delta}^{Vac-Vac}$ is the pathway for a zirconium atom to migrate from an initial site to a vacancy site.

For δ-ZrH_2, the migration barrier for hydrogen atoms in δ-ZrH_2 is smallest along the $H_{\delta}^{Oct-Oct-2}$, with a barrier value of 0.371 eV, while the migration barrier for hydrogen atom at the octahedral position along the $H_{\delta}^{Oct-Oct-1}$ path is significantly higher at 1.417 eV. In the presence of a hydrogen vacancy, the migration energy barrier for hydrogen atom diffusion to the vacancy ($H_{\delta}^{Vac-Vac}$) is 1.064 eV. Conversely, when there is a vacancy of zirconium atom, the migration of zirconium atom from its original position to the vacancy ($Zr_{\delta}^{Vac-Vac}$) shows a much larger potential barrier than all other paths followed by the movement of hydrogen atom, reaching 2.971 eV. The DP model aligns well with DFT results in terms of migration barrier curve and predicts migration energy values of 0.322 eV, 1.333 eV, 2.950 eV, and 1.039 eV for paths $H_{\delta}^{Oct-Oct-1}$, $H_{\delta}^{Oct-Oct-2}$, $Zr_{\delta}^{Vac-Vac}$, and $H_{\delta}^{Vac-Vac}$, respectively.

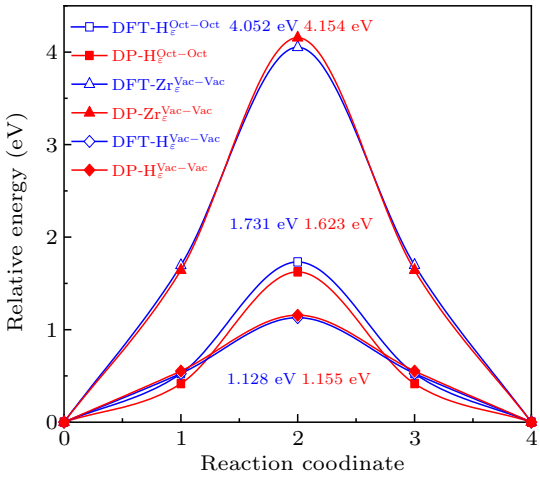


Fig. 8. Migration energy along different paths in ε-ZrH_2. $H_{\varepsilon}^{Oct-Oct}$ refers to the NEB pathway for a hydrogen atom migrating from an octahedral site to another octahedral site. $H_{\varepsilon}^{Vac-Vac}$ denotes the pathway of a hydrogen atom migrating from a tetrahedral site to a tetrahedral vacancy site. $Zr_{\varepsilon}^{Vac-Vac}$ represents the pathway for a zirconium atom to migrate from an initial site to a vacancy site.

For ε-ZrH_2, Hou *et al.*[64] investigated various migration paths of hydrogen atoms in the presence of hydrogen vacancies and identified T–T2–T1 (The hydrogen atom starts from the original position through the tetrahedral interstitial site and reaches the location of the excavated hydrogen atom, as a result, the original position turns into vacancy) as the most favorable fusion pathway. To facilitate the recognition of DP model of this pathway, we replicate the calculation of the transfer energy barrier in this study. The obtained result aligns with that of T–T2–T1, which represents the optimal fusion path. Furthermore, our DP model successfully reproduces this outcome (Fig. 9). Our calculations indicate a migration energy barrier value of 0.489 eV for the T–T2–T1 migration path, slightly higher than the value of 0.456 eV reported by Hou *et al.* Additionally, the DP model test yields a value of 0.519 eV. The results of ε-ZrH_2 are presented in Fig. 8. Of the three species, $Zr_{\varepsilon}^{Vac-Vac}$ has the highest transfer energy of 4.052 eV,

$H_{\varepsilon}^{Oct-Oct}$ has 1.731 eV, while $H_{\varepsilon}^{Vac-Vac}$ has the lowest transfer energy of 1.128 eV. The barrier heights obtained from the DP model align with the energy order predicted by the DFT calculations, with respective transfer energy of 4.154 eV for $Zr_{\varepsilon}^{Vac-Vac}$, 1.623 eV for $H_{\varepsilon}^{Oct-Oct}$, and 1.155 eV for $H_{\varepsilon}^{Vac-Vac}$. Hydrogen loss poses a significant challenge in implementing metal hydride neutron moderators in reactors. Thus, accurately characterizing hydrogen diffusion behavior is crucial for investigating hydrogen desorption kinetics.[65] The diffusion of hydrogen and zirconium discussed in this work can serve as a fundamental basis for investigating the kinetics of hydrogen desorption.

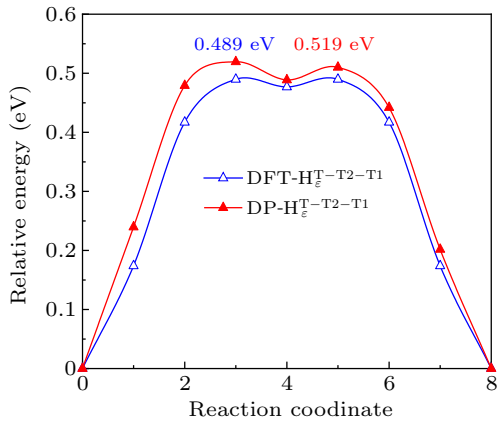


Fig. 9. CI-NEB pathways for hydrogen migration from tetrahedral site to tetrahedral site through tetrahedral site ($H_{\varepsilon}^{T-T2-T1}$) with related migration energy of H in the vicinity of a vacancy in ε-ZrH_2.

3.4. Threshold energy of displacement in ε-ZrH_2

In the research of radiation simulation, it is difficult to directly simulate the radiation with high-energy and high-current neutrons, so primary knock-on atoms (PKAs) with certain kinetic energy are usually used to simulate the cascade collision process. These PKAs refer to lattice atoms that gain some energy after being impacted by neutrons and subsequently impact the lattice atoms of materials. The radiation damage and anti-radiation properties of the material are studied by analyzing the changes in the material after the cascade collision. In the process of defect evolution, the threshold energy of displacement (E_d) is a crucial parameter, which plays a key role in the generation of PKA and the subsequent cascade process and is the basis for ensuring the cascade process and the correctness of the simulation results. To simulate the short-range interaction between atoms in the cascade process, we introduce Ziegler–Biersack–Littmark (ZBL) potential into the DP model which is represented as DP-ZBL. The DP model access ZBL potential has its interface in the DPMD-kit, and by adding keywords during training to activate the DP-Tab mode after preparing the Tab potential table file. Other training parameters remain unchanged. The specific methodological details can be found in Ref. [66]. Then, we calculate the threshold energy of displacement of zirconium and hydrogen in ε-ZrH_2 for the DP-ZBL model.

In this work, in the simulation, three-dimensional periodic boundary conditions are adopted, and the simulated crystal cell is the 20×20×20 supercell of ε-ZrH_2. The simulated configuration spans dimensions of 70 Å×70 Å×89 Å in the x, y, and z directions, encompassing a total of 4.8×10^4 atoms. The area surrounded by x from 8 Å to 62 Å, y from 8 Å to 62 Å, and z from 8 Å to 80 Å is set as an interior area. The simulations are all conducted at a temperature of 30 K. The system is first subjected to static relaxation by using the conjugate gradient method. Then, the entire simulated cell is subjected to dynamic relaxation of 1 ps by using the Nose–Hoover hot bath and pressure control method in the NPT ensemble, with time steps of 1 fs. After equilibration, in the radiation damage simulations, a canonical ensemble (NVT) is used for the outer layer of atoms and a microcanonical ensemble (NVE) is utilized for the inner section of atoms. The outer boundary region of the simulated crystal cell is controlled to maintain a lattice system temperature through the velocity calibration method. A zirconium or hydrogen atom near the center of the simulated crystal cell is randomly selected as the PKA. To obtain the minimum energy of displacement in each direction, the recoil energy increases from 0 in steps of 1 eV until a Frenkel-pair is first recognized, then, the recoil energy decreases in steps 0.1 eV to obtain a more accurate value. The minimum PKA energy corresponding to the generation of a stable Frenkel-pair is defined as the E_d of the atom in the chosen direction. The Wigner–Seitz method is adopted for defect analysis,[67] and the Wigner–Seitz primitive cell is constructed with the lattice atomic position at time $t = 0$. The system structure at a time of cascade collision is compared with the Wigner–Seitz primitive cell. If there are no atoms in the Wigner–Seitz primitive cell, the Wigner–Seitz primitive cell is said to be empty. If there are two or more atoms in a Wigner–Seitz primitive cell, the atom farther away from $t = 0$ is interstitial atom. We calculated the E_ds of zirconium and hydrogen along the direction of [100], [101], [111] and the calculation results are listed in Table 7.

Table 7. Calculation results of threshold energy of displacement (E_d) for Zr and H.

PKA atom	Direction	E_d (eV)
Zr	100	22.7
	101	21.5
	111	24.5
H	100	4.6
	101	5.2
	111	4.8

For the DP-ZBL, zirconium PKA has the largest E_d in the [111] direction, followed by the [100] direction, and the smallest E_d in the [101] direction, which are 24.5 eV, 22.7 eV, and 21.5 eV, respectively. The E_d of the hydrogen PKA is around 5 eV in all directions. In the [101] direction, E_d has a maximum value of 5.2 eV, followed by 4.8 eV in the [111]

direction, and a minimum value of 4.6 eV in the [100] direction. In general, the E_ds of hydrogen and zirconium in DP-ZBL exhibit minimal variation with direction, which is likely to be attributed to the bonding characteristics between ε-ZrH_2 atoms and the inherent symmetry of the crystal structure. The E_d of hydrogen varies in a range of 4 eV–6 eV, while the E_d of zirconium varies in a range of 21 eV–25 eV. The above results indicate that hydrogen has a lower threshold energy of displacement and is more likely to leave the initial position, which promotes the formation and diffusion of hydrogen defects, and also confirms the result that the defect formation energy and migration barrier of hydrogen are lower than those of zirconium defects. In conclusion, the molecular dynamics can be used to examine threshold displacement occurrences along three main crystallographic orientations in zirconium hydride. The predicted E_d values provide relevant parameters for modeling radiation damage in ZrH_2 in the future.

4. Discussion

From the above evaluation results, the potential of the ZrH_2 system developed in this work is satisfactory. The DP model can well describe the basic bulk properties of α-Zr, δ-ZrH_2, and ε-ZrH_2. In addition, this potential can accurately describe the point defects of ZrH_2 and the diffusion energy barrier of point defects, and the calculated results are in good agreement with the DFT results. The potential model proposed in this work serves as the foundation for comprehending the service performance of zirconium hydride as a neutron moderator material in nuclear reactors. This potential can be used to study the thermodynamic properties and defect kinetics of the ZrH_2 neutron moderator. Another important application of this potential is to study the diffusion of H atoms in ZrH_2 and the hydrogen loss behavior of H on the surface. The high-temperature radiation performance data of zirconium hydride are the basis to support its engineering application in micronuclear reactors, but the research in this area is very scarce. Describing the kinetics of hydrogen desorption during the diffusion release of hydrogen from zirconium hydride is the physical basis for characterizing its high-temperature thermal stability. Despite this, many questions in this field remain to be resolved, and the development of interatomic potentials and MD simulations, which will take place in the future, can provide insights into these questions. Considering the special phase structure of ε-ZrH_2, the we believe that this work is an important step in the development of the interatomic potential of ZrH_2 system. The current work still has some shortcomings. The influence of the threshold energy of displacement is dependent on the size of the simulation box and the time step. Nonetheless, the influence of these variables on the simulation results is not included in this specific simulation study. The discrepancy between DP models and experiments is limited by the inconsistencies between DFT calculations and experiments. In the subsequent research, we will focus on enhancing the fusion of multiple data, including experimental data, into the model training process to improve the ability of the potential to describe experimental results. In future work, we will use the DP model to continuously optimize the potential to address any problems that may arise. If more efficient and accurate potential models are proposed in the future, and more knowledge about the ZrH_2 system is gained from first-principles calculations and experimental results, then the potential should be further improved.

5. Conclusions

The deep learning potential method is employed to establish an accurate potential for ZrH_2 neutron moderator material. The results demonstrate that the developed potential accurately describes both pure zirconium and zirconium hydride. Firstly, for pure zirconium, the DP model effectively calculates various fundamental properties of α-Zr, including lattice constants, elastic constants, cohesive energy, equation of state, and surface energy. Regarding ZrH_2, the DP model exhibits high accuracy in determining the lattice constants, elastic constants, and equation of state for both δ-ZH_2 and ε-ZrH_2. Furthermore, the DP model successfully reproduces the point defect properties and diffusion behavior of hydrogen and zirconium in δ-ZH_2 and ε-ZrH_2. Additionally, by combining the DP model with ZBL potentials the DP-ZBL approach is utilized to compute the threshold energy values of displacement of hydrogen and zirconium in various orientations within ε-ZrH_2. The developed potential model effectively characterizes the defect properties in ZrH_2. Performing molecular dynamics simulations based on our potential model can significantly enhance our understanding of the evolution of radiation defects in ZrH_2 as a neutron moderator. The data obtained from these simulations can serve as a fundamental basis for further research on the evolution of radiation defects.

Data availability statement

The data that support the findings of this study are available from the corresponding author upon reasonable request.

Acknowledgement

Project supported by the Joint Fund of the National Natural Science Foundation of China – “Ye Qisun” Science Fund (Grant No. U2341251).

References

[1] Bickel P W and Berlincourt T G 1970 *Phys. Rev. B* **2** 4807
[2] Simnad M 1981 *Nucl. Eng. Des.* **64** 403

[3] Haslett R 1995 *Space nuclear thermal propulsion program*, Grumman Aerospace Corp TR PL-TR-95-1064, Bethpage, NY
[4] Narang P P, Paul G L and Taylor K N R 1977 *Journal of The Less-Common Metals* **56** 125
[5] Khoda-Bakhsh R and Ross D K 1982 *J. Phys. F: Metal Phys.* **12** 15
[6] Lanzani L and Ruch M 2004 *J. Nucl. Mater.* **324** 165
[7] Zhao Z, Morniroli J P, Legris A, Ambard A, Khin Y, Legras L and Blat-Yrieix M 2008 *Journal of Microscopy* **232** 410
[8] Wang Z, Garbe U, Li H, Harrison R P, Toppler K, Studer A J, Palmer T and Planchenault G 2013 *J. Nucl. Mater.* **436** 84
[9] Domain C, Besson R and Legris A 2002 *Acta Materialia* **50** 3513
[10] Zhu W, Wang R, Shu G, Wu P and Xiao H 2010 *J. Phys. Chem. C* **114** 22361
[11] Wang F and Gong H R 2012 *International Journal of Hydrogen Energy* **37** 12393
[12] Wang H, Chroneos A, Jiang C, *et al.* 2013 *Phys. Chem. Chem. Phys.* **15** 7599
[13] Lumley S C, Grimes R W, Murphy S T, Burr P A, Chroneos A, Chard-Tuckey P R and Wenman M R 2014 *Acta Mater.* **79** 351
[14] Olsson P A T, Massih A R, Blomqvist J, Alvarez Holston A M and Bjerkén C 2014 *Comput. Mater. Sci.* **86** 211
[15] Zhang P, Wang B T, He C H and Zhang P 2011 *Comput. Mater. Sci.* **50** 3297
[16] Mendelev M I and Ackland G J 2007 *Philosophical Magazine Letters* **87** 349
[17] Siripurapu R K, Szpunar B and Szpunar J A 2014 *Int. J. Nucl. Energy* **2014** 912369
[18] Noordhoek M J, Liang T, Chiang T W, Sinnott S B and Phillpot S R 2014 *J. Nucl. Mater.* **452** 285
[19] Lee B M and Lee B J 2014 *Metallurgical and Materials Transactions A: Physical Metallurgy and Materials Science* **45** 2906
[20] Thompson A P, Swiler L P, Trott C R, *et al.* 2015 *J. Comput. Phys.* **285** 316
[21] Shapeev A V 2016 *Multiscale Modeling and Simulation* **14** 1153
[22] Behler J and Parrinello M 2007 *Phys. Rev. Lett.* **98** 146401
[23] Bartók A P, Payne M C, Kondor R and Csányi G 2010 *Phys. Rev. Lett.* **104** 136403
[24] Chmiela S, Tkatchenko A, Sauceda H E, Poltavsky I, Schütt K T and Müller K R 2017 *Sci. Adv.* **3** e1603015
[25] Schütt K T, Kindermans P J, Sauceda H E, Chmiela S, Tkatchenko A and Müller K R 2017 *Advances in Neural Information Processing Systems* **30** 991
[26] Smith J S, Isayev O and Roitberg A E 2017 *Chem. Sci.* **8** 3192
[27] Han J, Zhang L, Car R and Weinan E 2018 *Commun. Comput. Phys.* **23** 629
[28] Zhang L, Han J, Wang H, Car R and Weinan E 2018 *Phys. Rev. Lett.* **120** 143001
[29] Zhang L, Han J, Wang H, Saidi W A and Weinan E 2018 *Advances in Neural Information Processing Systems* **31** 4436
[30] Wood M A and Thompson A P arXiv:1702.07042 [physics. comp-ph]
[31] Zhang L, Lin D Y, Wang H, Car R and Weinan E 2019 *Phys. Rev. Mater.* **3** 023804
[32] Jiang W, Zhang Y, Zhang L and Wang H 2021 *Chin. Phys. B* **30** 050706
[33] Wang Y, Zhang L, Xu B, Wang X Y and Wang H 2022 *Modelling and Simulation in Materials Science and Engineering* **30** 025003
[34] Wen T, Wang R, Zhu L, Zhang L, Wang H, Srolovitz D J and Wu Z 2021 *Npj Comput. Mater.* **7** 206
[35] Wang R, Ma X, Zhang L, Wang H, Srolovitz D J, Wen T and Wu Z 2022 *Phys. Rev. Mater.* **6** 113603
[36] Wang X, Wang Y, Zhang L, Dai F and Wang H 2022 *Nuclear Fusion* **62** 126013
[37] Pitike K C and Setyawan W 2023 *J. Nucl. Mater.* **574** 154183
[38] Zhang Y, Wang H, Chen W, Zeng J, Zhang L, Wang H and Weinan E 2020 *Comput. Phys. Commun.* **253** 107206
[39] Zheng J, Zhou X, Mao L, Zhang H, Liang J, Sheng J and Peng S 2015 *International Journal of Hydrogen Energy* **40** 4597
[40] Zhu X, Lin D Y, Fang Y J, Gao X Y, Zhao Y F and Song H F 2018 *Comput. Mater. Sci.* **150** 77
[41] Chattaraj D, Parida S C, Dash S and Majumder C 2014 *International Journal of Hydrogen Energy* **39** 9681
[42] Car R and Parrinello M 1985 *Phys. Rev. Lett.* **55** 2471
[43] Plimpton S 1995 *J. Comput. Phys.* **117** 1
[44] Wang H, Zhang L, Han J and Weinan E 2018 *Comput. Phys. Commun.* **228** 178
[45] Kohn W and Sham L J 1965 *Phys. Rev.* **140** A1133
[46] Hohenberg P and Kohn W 1964 *Phys. Rev.* **136** B864
[47] Perdew J P, Burke K and Ernzerhof M 1996 *Phys. Rev. Lett.* **77** 3865
[48] Kresse G and Furthmüller J 1996 *Phys. Rev. B* **54** 11169
[49] Kresse G and Furthmüller J 1996 *Comput. Mater. Sci.* **6** 15
[50] Zhou M, Fu B, Hou Q, Wu L and Pan R 2022 *J. Nucl. Mater.* **566** 153772
[51] Liyanage M, Reith D, Eyert V and Curtin W A 2022 *Phys. Rev. Mater.* **6** 063804
[52] Zhang S, Zhang X, Zhu Y, Zhang S, Qi L and Liu R 2012 *Comput. Mater. Sci.* **61** 42
[53] Ikehata H, Nagasako N, Furuta T, Fukumoto A, Miwa K and Saito T 2004 *Phys. Rev. B* **70** 174113
[54] Wang B T, Zhang P, Liu H Y, Li W D and Zhang P 2011 *J. Appl. Phys.* **109** 063514
[55] Hao Y J, Zhang L, Chen X R, Li Y H and He H L 2008 *J. Phys.: Conden. Matter* **20** 235230
[56] Zheng J, Zhang H, Zhou X, Liang J, Sheng L and Peng S 2014 *Adv. Condens. Matter Phys.* **2014** 929750
[57] Pearson W B and Vineyard G H 1958 *Physics Today* **11** 36
[58] Nitol M S, Dickel D E and Barrett C D 2022 *Acta Materialia* **224** 117347
[59] Fisher E S and Renken C J 1964 *Phys. Rev.* **135** A482
[60] Boer F R 1988 *Cohesion in metals: transition metal alloys*, Vol. 1 (North Holland)
[61] Tyson W R and Miller W A 1977 *Surf. Sci.* **62** 267
[62] Niedźwiedź K and Nowak B 1993 *J. Alloys Compd.* **194** 47
[63] Henkelman G, Uberuaga B P and Jónsson H 2000 *J. Chem. Phys.* **113** 9901
[64] Hou H, Pan Y, Bai G, Li Y, Murugadoss V and Zhao Y 2022 *Advanced Composites and Hybrid Materials* **5** 1350
[65] Vetrano J B 1971 *Nuclear Engineering and Design* **14** 390
[66] Wang H, Guo X, Zhang L, Wang H and Xue J 2019 *Appl. Phys. Lett.* **114** 244101
[67] Nordlund K and Averback R 1997 *Phys. Rev. B* **56** 2421